LANGMUIR

Article

pubs.acs.org/Langmuir

Mechanical Characterization of Ultralow Interfacial Tension Oil-in-Water Droplets by Thermal Capillary Wave Analysis in a Microfluidic Device

Guido Bolognesi,[†] Yuki Saito,[†] Arwen I. I. Tyler,[†] Andrew D. Ward,[‡] Colin D. Bain,[¶] and Oscar Ces*[,†]

[†]Department of Chemistry, Imperial College London, London SW7 2AZ, U.K.

[‡]Central Laser Facility, STFC, Harwell Oxford OX11 0QX, U.K.

[¶]Department of Chemistry, Durham University, Durham DH1 3LE, U.K.

Supporting Information

ABSTRACT: Measurements of the ultralow interfacial tension and surfactant film bending rigidity for micron-sized heptane droplets in bis(2-ethylhexyl) sodium sulfosuccinate−NaCl aqueous solutions were performed in a microfluidic device through the analysis of thermally driven droplet interface fluctuations. The Fourier spectrum of the stochastic droplet interface displacement was measured through bright-field video microscopy and a contour analysis technique. The droplet interfacial tension, together with the surfactant film bending rigidity, was obtained by fitting the experimental results to the prediction of a capillary wave model. Compared to existing methods for ultralow interfacial tension measurements, this contactless, nondestructive, all-optical approach has several advantages, such as fast measurement, easy implementation, cost-effectiveness, reduced amount of liquids, and integration into lab-on-a-chip devices.

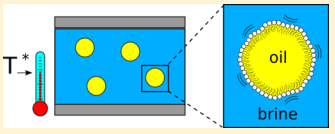

INTRODUCTION

Immiscible liquids with ultralow interfacial tensions (ULIFT), such as oil−water microemulsions and aqueous two-phase systems, are ubiquitous in a number of important applications in the oil industry (e.g., enhanced oil recovery) and environmental protection (e.g., oil pollution remediation), as well as the food and pharmaceutical industries. When the interfacial tension reaches values lower than 1 μN/m, classical techniques, such as the Wilhelmy plate and the pendant/sessile drop, are very difficult to apply. For those systems, the commonly used techniques are based on the analysis of either the steady-state deformation of droplets caused by external forces (e.g., spinning droplet tensiometry)[1] or droplet relaxation dynamics after cessation of the rotational flow field (e.g., relaxation time method).[2] Similarly, the interfacial tension can also be estimated by following the early breakup dynamics of elongated droplets subject to rotational flow fields (the so-called breaking-thread method).[3] Alternatively, the profile analysis of flat interfaces deformed either by the presence of single walls[4] or by continuous laser sources[5] can be used to measure such ultralow values of interfacial tension. Unfortunately, these methods require dedicated apparatus, and hence, they cannot be integrated into a lab-on-a-chip device with multiple functionalities. To this end, Tsai et al.[6] have recently introduced a microfluidic device for ultralow interfacial tensiometry where the interfacial tension is estimated by analyzing the dynamics of magnetic particles crossing a flat liquid interface. Although this microfluidic technique can effectively measure interfacial tension on the order of 0.1−1 μN/m, the precalibration of the particle magnetic susceptibility, the risk of interface contamination caused by these magnetic probes, and the requirements of low viscosity contrast between the liquid phases limit the applicability of this method. Furthermore, none of the mentioned methods can measure the bending rigidity of the fluid−fluid interface.

Laser manipulation of ULIFT oil−water interfaces within a microfluidic environment has recently attracted growing interest both experimentally[7−10] and theoretically.[11] Carefully chosen surfactant−oil−water systems can be used to lower the interfacial tension down to 1 μN/m or less. Under this condition, optical fields allow one to sculpt oil droplets into more complex shapes for manufacturing asymmetric solid particles,[7,8,12] to actuate flows in micron-sized liquid channels created by light[9] as well as to create user-defined three-dimensional nanofluidic networks.[10,13] In order to characterize and optimize emulsion systems for such applications, a simple and fast method for ULIFT measurements is highly desirable. A microfluidic approach offers the possibility of integrating the mechanical characterization of the ULIFT interfaces directly into the lab-on-a-chip devices, where these interfaces are optically manipulated, hence avoiding the need for a dedicated tensiometry apparatus (e.g., spinning droplet tensiometer).

At equilibrium, thermal motion causes stochastic fluctuations of the local position of the interface between two fluid phases.[14] The typical amplitude of this thermally driven capillary waves is on the order of $(k_bT/\gamma)^{1/2}$, where k_b is the Boltzmann constant, T is the absolute temperature, and γ is the interfacial tension. When γ is in the range from 0.1 to 1 μN/m, the fluctuation amplitudes are on the order of 100 nm, so conventional digital video microscopy can be used to detect the capillary waves at

Received: December 24, 2015
Revised: March 11, 2016
Published: March 16, 2016

DOI: 10.1021/acs.langmuir.5b04702
Langmuir 2016, 32, 3580−3586

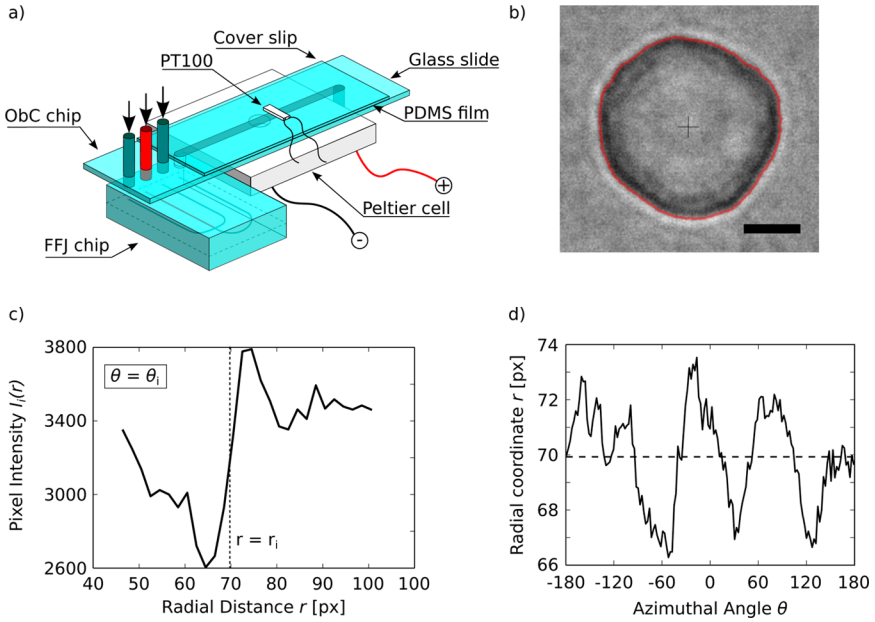

Figure 1. (a) Schematic of the microfluidic device for the manufacturing and characterization of ULIFT droplets. After generation in the flow focusing junction (FFJ) chip, droplets are transferred and stored in an observation chamber (ObC) chip, the temperature of which is controlled via a Peltier cell and a resistance thermometer (PT100). (b) Micrograph of a heptane droplet, in a 50 mM NaCl, 2 mM AOT aqueous solution at 26.3 °C, deformed by thermally induced capillary waves; see case iii in the text. The solid line represents the measured droplet interface profile. The scale bar is 5 μm. (c) Radial pixel intensity profile $I_i(r)$, averaged over the azimuthal angles from θ_i to θ_{i+1}. The inflection point r_i defines the radial coordinate of the interface point at the angle θ_i. (d) Measured interface profile (θ_i, r_i) with $i = 0, ..., N - 1$ for the droplet shown in panel b.

the interface between two phases. Such a direct visual observation of capillary waves for a phase-separated colloid–polymer system was performed through confocal microscopy by Aarts et al.,[15] thereby enabling the measurement of ultralow tension values. However, this approach required the use of a horizontally placed microscope in order to image the horizontal interface profile, and such a configuration is not suitable for lab-on-a-chip applications. Conversely, the analysis of the equilibrium thermal fluctuations, measured at the equatorial plane of lipid vesicles[16] and cell membranes,[17] enables the simultaneous measurements of the membrane interfacial tension and bending rigidity within a microfluidic environment by standard microscopy techniques. Despite these advantages, this method has never been used to characterize the interfacial properties of oil/water emulsion droplets.

In this work, we combined our microfluidic technique for the generation of monodisperse ultralow interfacial tension oil-in-water droplets with the analysis of thermal capillary waves, observed at the droplet equatorial plane through bright-field microscopy. By fitting the static fluctuation spectrum to the prediction of a capillary wave model, both the droplet interfacial tension and the surfactant film bending rigidity were measured. Although this method was validated for an oil–water–surfactant system close to the microemulsion phase transition, it could also be applied to other ULIFT systems, provided that a suitable capillary wave model is used (e.g., phase-separated colloid–polymer solutions, aqueous two-phase systems). Easy implementation, cost-effectiveness, fast measurement, absence of external probes, reduced amounts of liquid samples, and integration into microfluidic devices are the advantages of our approach with respect to other existing methods.

EXPERIMENTAL SECTION

Experimental Setup. The generation, transport, and storage of monodisperse ULIFT droplets were performed using a microfluidic platform described in our previous work[18] and briefly summarized here. Heptane (VWR, 99%) and an aqueous solution of bis(2-ethylhexyl) sodium sulfosuccinate (AOT) (Sigma-Aldrich, 98%) and sodium chloride (VWR, 99.6%) were used as dispersed and continuous phases, respectively. Droplets were generated in a glass flow-focusing junction device at room temperature ($T \simeq 21$ °C) and subsequently collected in a separate microfluidic chamber (Figure 1a). The latter was manufactured by plasma bonding a microscope glass slide to a 24 × 60 mm coverslip coated with a PDMS film 30 μm in thickness. The flow-focusing junction device (Dolomite 3200136) was fed with the aqueous (continuous) and oil (dispersed) phases by means of syringe pumps (WPI-Aladdin2-220). The flow rates of the aqueous and oil phases were 20 and 0.5 μL/min, respectively, and the resulting average droplet diameter was 15.5 ± 0.4 μm. After formation, droplets were transferred in the observation chamber, which was pre-equilibrated at the desired temperature through the thermal control unit. This was consisting of a 2 × 5 mm resistance thermometer (PT100 Class A) and a Peltier cell (Ferrotec) attached to the glass slide and coverslip of the observation chamber chip, respectively. The bottom wall of the chip was covered with a 2-mm-thick PDMS layer to be thermally isolated from the external environment. A 5 mm diameter hole was punched in the PDMS layer to avoid any optical aberration caused by the latter. The Peltier cell had a central 5 mm diameter hole to allow optical access to the chamber. A finite element analysis was performed with Comsol Multiphysics (COMSOL Ltd.) to estimate the temperature field in the observation chamber by assuming that heat enters the system from the Peltier module and leaves it through the external walls by natural convection. For a typical room temperature of 22 °C and an average chip temperature of 30 °C, the standard deviation of the temperature field in the observation chamber is about 0.3 °C. This value is a quantitative estimate for the uncertainty of the emulsion temperature measurements. Droplets were imaged using an inverted microscope (Olympus IX81) in bright-field mode, equipped with a 60× 0.7 NA objective and a 12-bit CCD camera (Q-Imaging Retiga EXi fast). The camera frame rate was varied between 1 and 10 fps. The scale factor m of the optical system was 0.109 μm per pixel.

DOI: 10.1021/acs.langmuir.5b04702
Langmuir 2016, 32, 3580–3586

Capillary Wave Model. The thermally driven fluctuations of a liquid−liquid interface about a reference plane $z = 0$ can be described through the normal displacement field $h(x,y)$. The Fourier transform of the static correlation function, defined as $g(x,y) = \langle h(x',y') h(x'+x,y'+y)\rangle$, gives the static fluctuation spectrum, which can be written as[16]

$$\langle |h(k_x,k_y)|^2\rangle = \frac{1}{A}\frac{k_bT}{\gamma k_\perp^2 + \kappa k_\perp^4} \quad (1)$$

where $h(k_x,k_y)$ is the Fourier transform of $h(x,y)$, defined as $\frac{1}{A}\int\int h(x,y)e^{-i(k_xx+k_yy)}\,dk_x\,dk_y$, $k_\perp$ is the amplitude of the wave vector (k_x,k_y) corresponding to the position vector (x, y), T is the temperature, γ the interfacial tension, κ the interface bending rigidity, A the interface area projected to the reference plane, and angled brackets denote the ensemble average. Since eq 1 describes the statics (not the dynamics) of the capillary waves, it does not contain any dynamic quantity (e.g., the liquid viscosities). Bright-field microscopy allows us to measure the interface deformation at the droplet equatorial plane only, so the observable fluctuation spectrum is[16]

$$\langle |h(k_x,y=0)|^2\rangle = \frac{k_bT}{2L_x\gamma}\left(\frac{1}{k_x} - \frac{1}{\sqrt{\frac{\gamma}{\kappa} + k_x^2}}\right) \quad (2)$$

where L_x is the droplet equatorial circumference.

The lifetime τ_m of the fluctuations decreases as the wavenumber increases. If at the higher wavenumbers τ_m is comparable to the camera exposure time τ, the corresponding interface deformations are averaged by the camera over the time τ. As a result, the fluctuation spectrum, measured at the higher modes, is no longer accurate. To correct the dynamic error caused by the camera, Pécréaux et al.[16] calculated the average of the static correlation function over the camera exposure time, thereby obtaining the following corrected prediction for the measured fluctuation spectrum

$$\langle |\bar{h}(k_x,y=0)|^2\rangle = \frac{k_bT}{4L_x\pi\eta}\int_{-\infty}^{+\infty}\frac{\tau_m^3}{\tau^2}\left[\frac{\tau}{\tau_m} + \exp\left(-\frac{\tau}{\tau_m}\right) - 1\right]dk_y \quad (3)$$

where the fluctuation lifetime is given by

$$\tau_m = \frac{4\eta}{\gamma k_\perp + \kappa k_\perp^3} \quad (4)$$

Equation 3 holds when the dispersed and continuous phases have the same dynamic viscosity η. In our system, the two phases have different viscosities, so we replaced the parameter η with an effective viscosity η_{eff} equal to $\eta_c\,(19\mu + 6)(2\mu + 3)(80\mu + 80)^{-1}$, where μ is the ratio between the continuous and dispersed phase dynamic viscosities η_c and η_d, respectively. The detailed derivation of η_{eff} is available in the Supporting Information (SI). To avoid any artifact caused by the camera dynamic error, we fitted the experimental data to eq 3 instead of eq 2. To ease the notation, in the following we will denote $\bar{h}(k_x,y=0)$, L_x, and k_x as $h(k)$, L, and k, respectively.

Interfacial Tension and Bending Rigidity Measurements. As the droplets reached the observation chamber chip, the flow was stopped and the droplets, at rest, were allowed to equilibrate at the chip temperature for a few minutes. The droplet interface profile was measured via image-processing analysis implemented in Python. The oil−water interface position was detected with subpixel precision on $N = L_{px}/3$ equally spaced points along the droplet interface, where $L_{px} = L/m$ is the droplet circumference in pixels. The following interface detection algorithm was adopted. After selecting an initial guess for the droplet center, the radial pixel intensity profile $I_i(r)$, averaged over the azimuthal angles from $\theta_i = 2\pi i/N$ to $\theta_{i+1} = 2\pi(i + 1)/N$, was calculated. The inflection point r_i of the pixel intensity distribution $I_i(r)$ was determined (Figure 1c) and assumed as the radial coordinate of the interface point at the angle θ_i. The same operations were repeated for i from 0 to $N - 1$. An example of the detected interface profile is shown in Figure 1b as a solid line overlapping the micrograph of a deforming droplet. The corresponding plot of the polar coordinates (θ_i, r_i) is reported in Figure 1d. Subsequently, the droplet interface profile was fitted to a circle. The center of the best-fitting circle was used as the new origin of the polar coordinate system, and the pixel intensity profiles $I_i(r)$, as well as the inflection points r_i, were calculated again with respect to this new center. Such an operation is required to avoid artifacts due to slight displacement of the droplet between two consecutive frames. The center of the best-fitting circle of one frame is used as an initial guess for the droplet center in the consecutive frame.

The interface fluctuation amplitude at the angle θ_i was defined as $u_i = r_i - R$, where R denotes the radius of the best-fitting circle. The discrete Fourier transform of the fluctuation displacements u_i was calculated and denoted as $U(k_n)$. The wavenumbers k_n are defined as $k_n = n\,N/R$ with $n \in [-N/2, N/2 - 1]$ if N is even or $n \in [-(N - 1)/2, (N - 1)/2]$ if N is odd. The experimental fluctuation spectrum $\langle |h(k_n)|^2\rangle$ was obtained by averaging the expression $|U(k_n)|^2/N^2$ over 200 frames. Finally, both the interfacial tension and the bending rigidity were obtained by fitting the experimental spectrum $\langle |h(k_n)|^2\rangle$ to eq 3.

The absolute errors of the measured interfacial tension and bending rigidity were calculated as 3 times the corresponding fit parameter uncertainties. To confirm the reproducibility of the results, we verified that three consecutive measurements for the same droplet at constant temperature returned interfacial tension and bending rigidity values within the corresponding absolute errors.

To conclude, it is worth reporting that, even though a third surfactant-rich microemulsion phase should coexist with the excess oil and water phases between the critical end point temperatures, such a third phase could not be observed in our experiments.

Fitting Procedure. The first five modes (i.e., k_0, k_1, ..., k_4) were not included in the fit, since at these wavenumbers the assumption of a planar interface is no longer valid.[16] The higher modes must also be excluded from the fit because of artifacts caused by the image pixelization and the finite lateral spatial resolution of the microscope. Due to the pixelization of the interface position in the direction parallel to the interface, we ignored any fluctuations wavelengths shorter than 5 pixels. Artifacts due to the microscope lateral spatial resolution d_{x-y} are avoided by disregarding fluctuations wavelengths smaller than $5d_{x-y}$. Consequently, the experimental fluctuation spectrum $\langle |h(k_n)|^2\rangle$ was fitted to eq 3 in the range $[k_5, k_{max}]$, where $k_{max} = \frac{2\pi}{5\,\max(m,d_{x-y})}$. The validity of the arbitrarily defined threshold k_{max} was confirmed by the experimental results, as discussed later.

The resolution of the interface position measurement in the direction orthogonal to the interface depends on several parameters, such as the image pixelization, the noise level of the camera, the exposure time, the microscope lamp intensity, and the objective numerical aperture. This resolution was experimentally measured by tracking the interface of a rigid droplet whose interfacial fluctuation amplitudes are on the order of nanometers or lower, thereby inaccessible to a bright-field microscope. The resulting fluctuation spectrum is a constant value ε, which defines the level of the random background noise in the Fourier domain. As a result, the experimental fluctuation spectra $\langle |h(k_n)|^2\rangle$ are fitted to eq 3 only in the range of wavenumbers where $\langle |h(k_n)|^2\rangle > \varepsilon$.

RESULTS AND DISCUSSION

Figure 2 shows the fluctuation spectra, excluding the first five modes, for heptane droplets in (i) 4 mM AOT aqueous solution at 21.0 °C (squares), (ii) 2 mM AOT and 50 mM NaCl aqueous solution at 26.6 °C (triangles), and (iii) 2 mM AOT and 50 mM NaCl aqueous solution at 26.3 °C (circles). The camera exposure time was 0.01 ms. The inset in the figure shows the normalized distributions of the fluctuation amplitudes for the three droplets together with the best-fitting Gaussian curves. For case i, the droplet interfacial tension is about 1 mN/m. Consequently, the expected fluctuation amplitudes were well below the localization precision, and

DOI: 10.1021/acs.langmuir.5b04702
Langmuir 2016, 32, 3580−3586

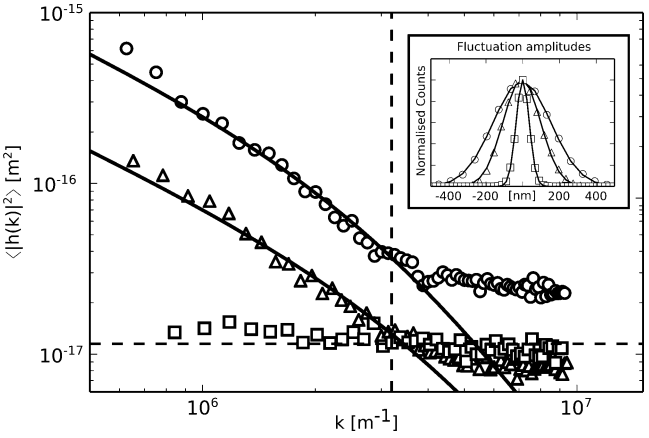

Figure 2. Fluctuation spectra for "rigid" (squares) and "soft" (circles and triangles) heptane droplets. The solid lines are the curves best fitting the experimental data for $k < k_{max}$ (vertical dashed line) and $\langle |h(k_n)|^2 \rangle > \varepsilon$ (horizontal dashed line). The normalized distributions of the interface displacements are shown in the inset together with the best-fitting Gaussian curves.

any measured interface displacement was just due to random noise. The droplet was hence rigid with a perfectly spherical shape. The corresponding standard deviation of the fluctuation distribution, which is about 36 nm (see inset Figure 2), provides a quantitative estimate for the resolution of our interface tracking method. Such a resolution can be reduced to 11 nm (that is $^1/_{10}$ of the pixel size) if the exposure time is increased to 0.1 ms. The spectrum of the rigid droplet is almost flat with a mean value of $\varepsilon \simeq 1.2 \times 10^{-17}$ m^2 (horizontal dashed line in figure). This spectrum represents the signal of the random background noise in the Fourier domain. The noise level ε is reduced to 1.1×10^{-18} m^2 when the camera exposure time is increased to 0.1 ms. As already mentioned, the experimental fluctuation spectra are fitted to eq 3 only in the range of wavenumbers where the squared amplitude of the fluctuations is higher than ε. This condition sets the upper limit of the range of interfacial tension that can be measured by our system to a few μN/m (see the SI). It is worth noting that, according to eqs 2 and 3, ε depends on the droplet radius. However, the microfluidic approach allowed us to generate a monodisperse droplet population, so such a dependence can be neglected. In cases ii and iii, 50 mM NaCl was added to 2 mM AOT aqueous phase. This AOT concentration is approximately 4 times the critical microemulsion concentration ($c\mu c$) for the examined system[19] (namely, $c\mu c \simeq 0.5$ mM), so surfactant aggregates in the form of microemulsions (either w/o or o/w) could be formed. At this salt concentration, it is known[19] that the heptane−brine−AOT system undergoes a microemulsion phase transition at approximately 26 °C and the oil−water interfacial tension decreases to ultralow values. Under these conditions, the droplets lost their spherical shape, and their interfaces were deformed by the thermal capillary waves, as shown in Figure 1b. For case ii, the standard deviation of the fluctuation distributions σ_A was 101 nm, and the best-fitting parameters of interfacial tension and bending rigidity were $\gamma = 0.50 \pm 0.09$ μN/m and $\kappa = 4.0 \pm 1.8 k_bT$, respectively. For case iii, higher interface fluctuation amplitudes were detected ($\sigma_A = 157$ nm) and the measured interfacial tension and bending rigidity were $\gamma = 0.12 \pm 0.02$ μN/m and $\kappa = 2.0 \pm 0.5 k_bT$, respectively. The vertical dashed line in Figure 2 represents the maximum detectable wavenumber $k_{max} = \frac{2\pi}{5 \max(m, d_{x-y})} = 3.9 \times 10^6 \text{m}^{-1}$, where $m = 0.109$ μm/px is the microscope scale factor and d_{x-y} is the microscope spatial resolution. The latter was estimated by using the Abbe formula $d_{x-y} = 0.5\ \lambda/NA$ with $\lambda = 550$ nm. As anticipated, at wavenumbers higher than k_{max}, the power spectra of the soft droplets depart from the theoretical prediction (solid lines). Further validation of our calculation of k_{max} is reported in the SI.

Our microfluidic platform allows us to control the emulsion temperature and, hence, to tune the interfacial tension of the droplets.[13] We thus carried out more than 100 measurements over heptane droplets in 2 mM AOT and 50 mM NaCl aqueous solution under varying temperature conditions. The resulting interfacial tension values varied over a range of a few tens of nN/m to a few μN/m. The standard deviation σ_A of the interface fluctuation distribution (see inset of Figure 2) is a measure of the typical fluctuation amplitude, and as such, it is expected to scale linearly with $\sqrt{k_bT/\gamma}$. Figure 3 shows the correlation between σ_A and $\sqrt{k_bT/\gamma}$ for our measurements. This plot is well fitted by a linear relation $\sqrt{k_bT/\gamma} = a\sigma_A$ with fitting parameter $a = 1.21 \pm 0.06$. Our measurements of interfacial tensions and interfacial fluctuation amplitudes thus follow the expected scaling law. It is also worth highlighting the correlation between the interfacial tension and the droplet equatorial radius R, shown in the left inset of Figure 3 for a single droplet. The droplet shape depends on the Bond number, Bo, which can be defined as $\Delta\rho g R_0^2/\gamma$, where $\Delta\rho$ is the density contrast between the two liquid phases, R_0 is the undeformed droplet radius, and g the gravitational constant. Hence, Bo represents the ratio of the buoyancy force, which pushes the droplet against the top wall of the channel, and the capillary force, which opposes the deformation of the droplet interface. For a monodisperse droplet population, larger equatorial radii correspond to higher deformations and thus lower interfacial tension (see right inset in Figure 3). This trend is confirmed by our experimental data. For a droplet diameter

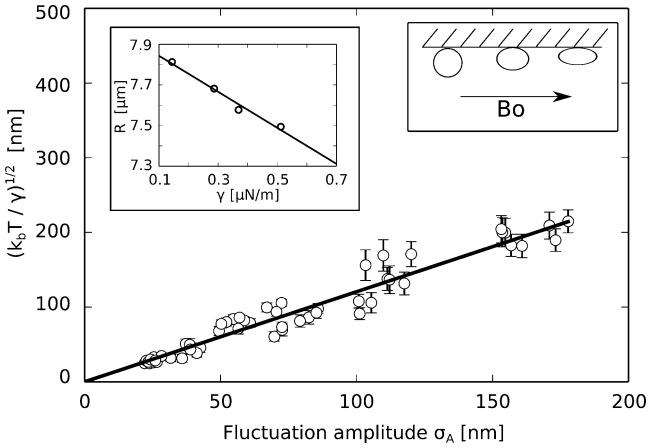

Figure 3. Fluctuation distribution σ_A scales linearly with $(k_bT/\gamma)^{1/2}$. The left inset shows the anticorrelation between the droplet radius and the interfacial tension, due to the balance between capillary and buoyancy arising from gravity force, assuming volume remains constant. A schematic cartoon (right inset) shows how increasing droplet deformations at higher Bond numbers (i.e., lower γ) result in larger droplet equatorial radii. The droplet deformations are greatly exaggerated for illustration purpose.

DOI: 10.1021/acs.langmuir.5b04702
Langmuir 2016, 32, 3580−3586

of 15 μm and interfacial tensions ranging from 0.1 to 1 μN/m, *Bo* varies between 0.2 and 2. As a result, the average droplet shapes only slightly deviate from a sphere, and hence, the buoyancy-induced droplet deformations have no effect on the interface fluctuation analysis.

Let us now consider the measurements of bending rigidity of the monolayer surfactant film coating the oil droplets. In Figure 4 the values of bending rigidity are plotted against those of

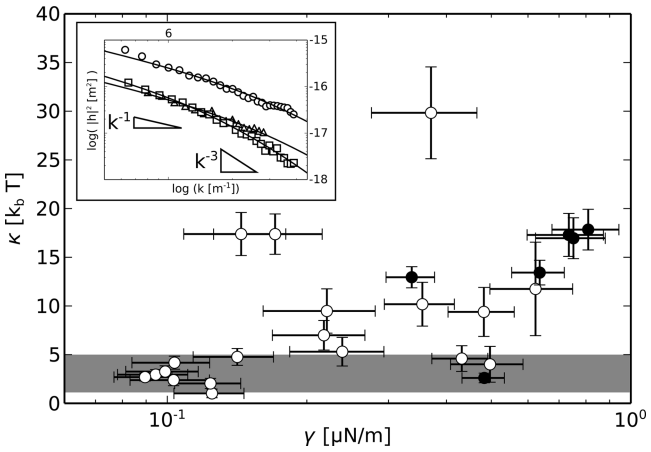

Figure 4. Correlation between the droplet interfacial tension γ and the AOT film bending rigidity κ. The droplet interface motion was tracked by using inverted microscopes equipped with 0.7 NA (white circles) and 1.4 NA (black circles) objectives. The gray area represents the range of values for the AOT film bending rigidity previously reported in the literature.[20,21] The inset shows the fluctuation spectra (obtained with a 0.7 NA objective) and the corresponding best-fitting curves for three droplets with increasing κ: 2.0k_bT (circles), 11.7k_bT (triangles), and 29.8k_bT (squares). The camera exposure times were 0.01 ms (circles and triangles) and 0.1 ms (squares). These spectra show a crossover from a scaling law k^{-1} at low wavenumbers, where the amplitude mainly depends on γ, to a scaling law k^{-3} at the high wavenumbers, where the amplitude mainly depends on κ.

interfacial tension. This plot shows two unexpected results: (i) at the higher interfacial tensions, the fitted values of κ are outside the range of $(0.5-5)k_bT$ (gray area in the figure) in which literature data of AOT film bending rigidity measurements fall[20,21] and (ii) the bending rigidity κ and the interfacial tension γ are positively correlated. The inset of Figure 4 shows the fluctuation spectra for three representative droplets with increasing bending rigidity. The corresponding fitted values for γ and κ were $\gamma = 0.12 \pm 0.02$ μN/m, $\kappa = (2.0 \pm 0.5)k_bT$ (circles); $\gamma = 0.62 \pm 0.13$ μN/m, $\kappa = (11.7 \pm 0.5)k_bT$ (triangles); and $\gamma = 0.37 \pm 0.09$ μN/m, $\kappa = (29.8 \pm 0.5)k_bT$ (squares). For wavenumbers $k \ll \sqrt{\gamma/\kappa}$, eq 2 can be approximated as $\langle |h(k)|^2 \rangle \simeq (k_bT)/(2L\gamma k)$, so the fluctuation spectrum depends mainly on the interfacial tension and it scales as k^{-1}. On the other hand, for wavenumbers $k \gg \sqrt{\gamma/\kappa}$, eq 2 reduces to $\langle |h(k)|^2 \rangle \simeq (k_bT)/(4L\kappa k^3)$, and the bending rigidity κ controls the fluctuation spectrum, which scales as k^{-3}. The crossover between the two regimes could be observed in the experimental spectra shown in the inset of Figure 4. Since the bending rigidity affects the interface fluctuations at the highest wavenumbers, artifacts due to the finite spatial resolution of the optical system could possibly compromise the accurate measurement of κ. For that reason, additional experiments were performed using an optical system with higher spatial resolution. A Nikon microscope equipped with a 1.4 NA oil immersion objective (see the SI for details) allowed us to fit the experimental fluctuation spectra up to $k_{max} = 6.4 \times 10^6$ m^{-1}, thereby increasing the examined wavenumber range almost by 65%. The corresponding results are shown in Figure 4 as black circles, and they confirmed the same trend of the previous data, thereby ruling out any issue related to an inadequate spatial resolution of the optical system. Possible inaccurate measurements of the bending rigidity due to the camera dynamic error are avoided by fitting the experimental spectra to eq 3 instead of eq 2. Moreover, artifacts ascribable to either the interface tracking algorithm or the fitting procedure were also excluded by performing test experiments where the bending rigidity of DOPC giant unilamellar vesicle membranes was measured and compared to the data available in the literature (data shown in the SI).

Since the positive correlation between γ and κ cannot be explained by any artifacts introduced by our experimental approach, we suggest a possible physical mechanism that can account for the observed behavior. For $\gamma = 0.1$ μN/m and $\kappa = k_bT$, the fluctuation lifetime τ_m at the examined wavenumbers is on the order of few milliseconds. Since fluctuations occur at constant droplet volume, the total interface area is not constant. If the area expands faster than the time required for surfactant to diffuse and cover the new interface, the local interfacial tension is higher than the equilibrium value γ_0. This results effectively in an interfacial tension dependent on the wavenumber: $\gamma(k_\perp) = \gamma_0 + \gamma_1(k_\perp)$. In that respect, the parameter κ in eq 1 accounts for the film bending rigidity as well as the term $\gamma_1(k_\perp)$. Equation 1 can be thus rewritten as

$$\langle |h(k_x,k_y)|^2 \rangle = \frac{1}{A}\frac{k_bT}{(\gamma_0 + \gamma_1(k_\perp))k_\perp{}^2 + \kappa_0 k_\perp{}^4} = \frac{1}{A}\frac{k_bT}{\gamma_0 k_\perp{}^2 + (\gamma_1(k_\perp)k_\perp{}^{-2} + \kappa_0)k_\perp{}^4} \quad (5)$$

with κ_0 being the actual film bending rigidity. So, the high values of the fitting parameter κ could be due to the term $\gamma_1(k_\perp)k_\perp{}^{-2}$ instead of κ_0, which is on the order of k_bT. Such a mechanism could also explain the positive correlation between γ and κ. As the interfacial tension increases, the measured interface fluctuations are of lower amplitude but are faster, thereby possibly limiting the amount of surfactant diffused to the interface. For a given wavenumber, this could lead to the increase of the local interfacial tension and, thus, of the term γ_1.

Finally, we validated our method by measuring the interfacial tensions of heptane droplets in 51.2 mM NaCl and 2 mM AOT aqueous solution at varying temperatures. Figure 5 shows the comparison between our interfacial tension measurements (gray circles) and those obtained by Aveyard et al. under the same conditions through spinning droplet tensiometry[19] (white circles). The good agreement between these two sets of data demonstrates that our method is capable of reproducing the expected trend of the interfacial tension against temperature. At a given salt concentration, the droplet interfacial tension reaches a minimum at the so-called phase inversion temperature (PIT). Spinning droplet tensiometry measurements near the PIT are difficult to perform because the ULIFT leads to the onset of artifacts (e.g., dumbbell- and dog-bone-shaped droplets) as well as hydrodynamic instabilities that eventually cause the droplet breakup. Our microfluidic method has no such disadvantages, but instead, its sensitivity and precision increase as temperature approaches the PIT, since lower

DOI: 10.1021/acs.langmuir.5b04702
Langmuir 2016, 32, 3580−3586

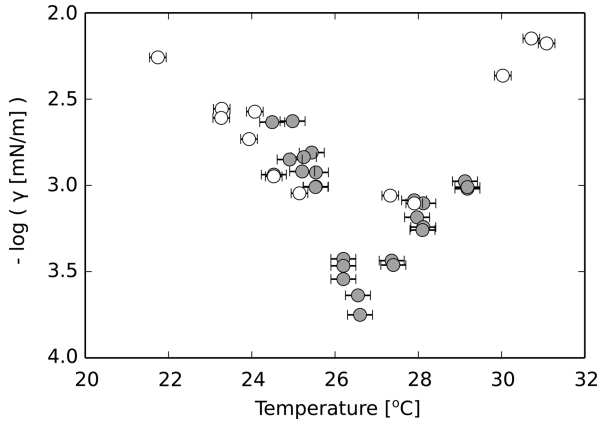

Figure 5. Variation of interfacial tension with temperature. The results from microfluidic tensiometry (gray circles) are in good agreement with those obtained through spinning droplet tensiometry[19] (white circles). The error bars are ±0.2 °C for the spinning droplet tensiometry data[22] and ±0.3 °C for the microfluidic tensiometry data.

interfacial tensions correspond to larger fluctuation amplitudes and, hence, higher signal-to-noise ratios. Furthermore, in spinning droplet tensiometry the density ratio between the dispersed and the continuous phases has to be lower than unity, whereas our microfluidic approach can measure the interfacial properties of droplets either lighter or heavier than the surrounding medium. Finally, the time required for the droplet shape to equilibrate during spinning droplet measurements can be quite long (up to 1 h) due to the slow droplet dynamics in the ULIFT regime. Conversely, micron-sized droplets, enclosed in a temperature-controlled microfluidic environment, rapidly reach the thermal equilibrium, and data acquisition for thermal capillary wave analysis is hence very fast (i.e., a few minutes).

Since our platform allows for the rapid evaluation of the droplet interfacial properties under varying conditions of temperature and salinity level, the proposed method is particularly useful for the characterization of those microemulsion systems for which the phase behavior is unknown and for which the physical conditions for the phase inversion have to be determined. Our technique should also allow for the characterization of the interfacial properties of other ULIFT systems (e.g., phase-separated colloid−polymer solutions,[23] all-aqueous polymer solutions[24]) as long as the interface fluctuation amplitudes are larger than the optical resolution of the microscope (namely, γ lower than a few μN/m) and an appropriate capillary wave model is used.

SUMMARY

In conclusion, in this paper we have presented a microfluidic technique for the measurement of the interfacial tension of oil-in-water droplets over a range from a few tens of nN/m to a few μN/m. The bending rigidity of the surfactant film, formed at the oil−water interface, was also determined. The Fourier spectrum of the droplet interface displacements was measured via bright-field digital video microscopy and fitted to the theoretical prediction for the thermal-driven fluctuations of a fluid membrane with the interfacial tension γ and the bending rigidity κ as the fitting parameters. The standard deviation of the fluctuation amplitudes was also measured and demonstrated to scale linearly with $(k_bT/\gamma)^{1/2}$. The fitting parameter κ was found to be positively correlated to γ. We hypothesize that at the higher wavenumbers the equilibrium surfactant surface coverage might not be reached on the time scale of the interface expansion. As a consequence, the dynamic interfacial tension depends on the fluctuation wavenumber, thereby leading to an additional term in the model parameter κ. Artifacts in the experimental method were ruled out by comparing the measurements obtained through optical setups with different spatial resolutions. The bending rigidity of DOPC giant unilamellar vesicles was also measured and compared to literature data. Our microfluidic technique was finally validated by measuring the interfacial tension for a heptane−AOT−NaCl−water system at varying temperatures and comparing our results with the corresponding spinning droplet tensiometry data available in the literature.

Compared to existing techniques for ULIFT measurements, our method has several advantages, including fast measurement, absence of external probes, easy implementation, reduced amount of liquids, and integration into lab-on-a-chip devices. As a consequence, this technique will prove very useful for the rapid characterization and optimization of ULIFT emulsion systems for both traditional applications, such as surfactant-enhanced oil recovery,[25] and more recent applications, such as flow actuation in micron-sized liquid channels created by light,[9] optical sculpture of micron-sized droplets[7] for the synthesis of asymmetric solid particles,[12] and optical generation and manipulation of nanofluidic networks.[10,13]

ASSOCIATED CONTENT

Supporting Information

The Supporting Information is available free of charge on the ACS Publications website at DOI: 10.1021/acs.langmuir.5b04702.

Further details on the microfluidic tensiometry technique and the results of control experiments (PDF)

AUTHOR INFORMATION

Corresponding Author

*E-mail: o.ces@imperial.ac.uk.

Notes

The authors declare no competing financial interest.

ACKNOWLEDGMENTS

We are pleased to thank Dr. P. Cicuta, Dr. N. J. Brooks, Dr. A. M. Howe, and all the members of the Optonanofluidics research team for interesting discussions. We also thank K. Karamdad and N. L. C. McCarthy for providing microscopy videos of giant unilamellar vesicle membranes. This work was supported by EPSRC grants EP/I013342/1, EP/K503733/1 and EP/G00465X/1.

REFERENCES

(1) Princen, H.; Zia, I.; Mason, S. Measurement of interfacial tension from the shape of a rotating drop. *J. Colloid Interface Sci.* **1967**, *23*, 99−107.

(2) Scholten, E.; Sagis, L. M.; van der Linden, E. Effect of bending rigidity and interfacial permeability on the dynamical behavior of water-in-water emulsions. *J. Phys. Chem. B* **2006**, *110*, 3250−3256.

(3) de Hoog, E. H.; Lekkerkerker, H. N. Measurement of the interfacial tension of a phase-separated colloid-polymer suspension. *J. Phys. Chem. B* **1999**, *103*, 5274−5279.

(4) Aarts, D. G. A. L.; van der Wiel, J. H.; Lekkerkerker, H. N. W. Interfacial dynamics and the static profile near a single wall in a model colloid-polymer mixture. *J. Phys.: Condens. Matter* **2003**, *15*, S245.

DOI: 10.1021/acs.langmuir.5b04702
Langmuir 2016, 32, 3580−3586

(5) Mitani, S.; Sakai, K. Measurement of ultralow interfacial tension with a laser interface manipulation technique. *Phys. Rev. E: Stat. Phys., Plasmas, Fluids, Relat. Interdiscip. Top.* **2002**, *66*, 031604.
(6) Tsai, S. S.; Wexler, J. S.; Wan, J.; Stone, H. A. Microfluidic ultralow interfacial tensiometry with magnetic particles. *Lab Chip* **2013**, *13*, 119−125.
(7) Ward, A. D.; Berry, M. G.; Mellor, C. D.; Bain, C. D. Optical sculpture: controlled deformation of emulsion droplets with ultralow interfacial tensions using optical tweezers. *Chem. Commun.* **2006**, 4515−4517.
(8) Ward, A.; Berry, M.; Ash, P.; Woods, D.; Bain, C. The polymerisation of emulsion droplets deformed using laser tweezers to create microscopic polymer particles. *CLF Ann. Rep.* **2006**, 199−201.
(9) Delville, J.-P.; de Saint Vincent, M. R.; Schroll, R. D.; Issenmann, B.; Lasseux, D.; Zhang, W. W.; Brasselet, E.; Chraibi, H.; Wunenburger, R. Laser microfluidics: fluid actuation by light. *J. Opt. A: Pure Appl. Opt.* **2009**, *11*, 034015.
(10) Woods, D. A.; Mellor, C. D.; Taylor, J. M.; Bain, C. D.; Ward, A. D. Nanofluidic networks created and controlled by light. *Soft Matter* **2011**, *7*, 2517−2520.
(11) Tapp, D.; Taylor, J. M.; Lubansky, A. S.; Bain, C. D.; Chakrabarti, B. Theoretical analysis for the optical deformation of emulsion droplets. *Opt. Express* **2014**, *22*, 4523−4538.
(12) Ward, A. D.; Bain, C. D.; Mellor, C. D. Droplet deformation. US Patent 8,183,540, 2012.
(13) Bolognesi, G.; Hargreaves, A.; Ward, A. D.; Kirby, A. K.; Neil, M.; Bain, C. D.; Ces, O. Microfluidic generation and optical manipulation of ultra-low interfacial tension droplets. *Proc. SPIE* **2015**, 95200B−95200B.
(14) v. Smoluchowski, M. Molekular-kinetische Theorie der Opaleszenz von Gasen im kritischen Zustande, sowie einiger verwandter Erscheinungen. *Ann. Phys. (Berlin, Ger.)* **1908**, *330*, 205−226.
(15) Aarts, D. G. A. L.; Schmidt, M.; Lekkerkerker, H. N. W. Direct visual observation of thermal capillary waves. *Science* **2004**, *304*, 847−850.
(16) Pécréaux, J.; Döbereiner, H.-G.; Prost, J.; Joanny, J.-F.; Bassereau, P. Refined contour analysis of giant unilamellar vesicles. *Eur. Phys. J. E: Soft Matter Biol. Phys.* **2004**, *13*, 277−290.
(17) Evans, J.; Gratzer, W.; Mohandas, N.; Parker, K.; Sleep, J. Fluctuations of the red blood cell membrane: relation to mechanical properties and lack of ATP dependence. *Biophys. J.* **2008**, *94*, 4134−4144.
(18) Bolognesi, G.; Hargreaves, A.; Ward, A. D.; Kirby, A. K.; Bain, C. D.; Ces, O. Microfluidic generation of monodisperse ultra-low interfacial tension oil droplets in water. *RSC Adv.* **2015**, *5*, 8114−8121.
(19) Aveyard, R.; Binks, B. P.; Clark, S.; Mead, J. Interfacial tension minima in oil-water-surfactant systems. Behaviour of alkane-aqueous NaCl systems containing aerosol OT. *J. Chem. Soc., Faraday Trans. 1* **1986**, *82*, 125−142.
(20) Binks, B.; Kellay, H.; Meunier, J. Effects of alkane chain length on the bending elasticity constant k of aot monolayers at the planar oil-water interface. *EPL* **1991**, *16*, 53.
(21) Huang, J.; Milner, S.; Farago, B.; Richter, D. *Physics of Amphiphilic Layers*; Springer, 1987; pp 346−352.
(22) Binks, B. P. Ultralow interfacial tensions and microemulsion formation in oil−water−surfactant systems. Ph.D. thesis, University of Hull, 1986.
(23) Jamie, E.; Davies, G.; Howe, M.; Dullens, R.; Aarts, D. Thermal capillary waves in colloid-polymer mixtures in water. *J. Phys.: Condens. Matter* **2008**, *20*, 494231.
(24) Liu, Y.; Lipowsky, R.; Dimova, R. Concentration dependence of the interfacial tension for aqueous two-phase polymer solutions of dextran and polyethylene glycol. *Langmuir* **2012**, *28*, 3831−3839.
(25) He, L.; Lin, F.; Li, X.; Sui, H.; Xu, Z. Interfacial sciences in unconventional petroleum production: from fundamentals to applications. *Chem. Soc. Rev.* **2015**, *44*, 5446−5494.

DOI: 10.1021/acs.langmuir.5b04702
Langmuir 2016, 32, 3580−3586